AIP | The Journal of Chemical Physics

Rotationally resolved near-threshold photoionization of the 1b 1 valence orbital of H2O and D2O

M.-T. Lee, Kwanghsi Wang, and V. McKoy

Citation: The Journal of Chemical Physics **97**, 3108 (1992); doi: 10.1063/1.462998
View online: http://dx.doi.org/10.1063/1.462998
View Table of Contents: http://scitation.aip.org/content/aip/journal/jcp/97/5?ver=pdfcov
Published by the AIP Publishing

Rotationally resolved near-threshold photoionization of the $1b_1$ valence orbital of H_2O and D_2O

M.-T. Lee,[a] Kwanghsi Wang, and V. McKoy
Arthur Amos Noyes Laboratory of Chemical Physics,[b] *California Institute of Technology, Pasadena, California 91125*

(Received 10 April 1992; accepted 11 May 1992)

Results of theoretical studies of rotationally resolved ion distributions for near-threshold photoionization of the $1b_1$ valence orbital of H_2O and D_2O are reported and compared with measured spectra. Agreement between the calculated and measured spectra is very encouraging. The calculated and measured spectra reveal both type *a* and type *c* transitions in contrast to type *c* transitions only expected in an atomiclike picture. Type *a* transitions arise from odd (mainly *p* wave) angular momentum components of the photoelectron matrix elements which are due to *l* mixing in the electronic continua. These type *a* transitions are quite molecular in origin and are similar to nonatomiclike transitions seen in resonance enhanced multiphoton ionization of excited states of diatomic molecules. Useful rotational selection rules are also obtained.

I. INTRODUCTION

Rotationally resolved photoelectron spectroscopy provides a useful probe of molecular electronic states and the photoionization dynamics of these states.[1-3] Such rotationally resolved photoelectron spectra have been studied using the technique of zero-kinetic-energy (ZEKE) photoelectron detection[3] and time-of-flight measurements[2] for a wide range of systems. With ZEKE photoelectron detection, the spectral resolution is essentially that of the laser bandwidth (~ 0.1 cm^{-1}) and hence provides rotational resolution for larger molecular ions.[3] Of particular interest to the present studies are the rotationally resolved ZEKE pulsed-field-ionization (PFI) spectra of H_2O and D_2O reported by Tonkyn *et al.*[4] for single-photon ionization of the $1b_1$ orbital with a coherent vacuum ultraviolet radiation source. These spectra can be assigned to two types of rotational transitions, corresponding to specific changes in K_a and K_c. Here K_a and K_c are the projections of the total angular momentum (except spin) along the principal *a* and *c* axes, respectively. Most of the strong spectral lines could be classified as type *c* rotational transitions ($\Delta K_a = \text{odd}, \Delta K_c = \text{even}$), but type *a* transitions ($\Delta K_a = \text{even}, \Delta K_c = \text{odd}$) are also clearly evident. These type *a* transitions cannot be accounted for simply on the basis of an atomiclike model for photoionization of this $1b_1$ orbital.[5] A systematic investigation of the underlying photoionization dynamics of these ZEKE photoelectron spectra is clearly desirable.

In a recent study using multichannel quantum defect theory (MQDT), Child and Jungen[5] predicted that only type *c* transitions are allowed for photoionization of the $1b_1$ orbital of ground state H_2O. Gilbert and Child[6] further proposed a rotational autoionization mechanism, based on polarization-induced quasiautoionizing state mixing between the $1b_1 \rightarrow nd$ and $1b_1 \rightarrow np$ Rydberg series, in an effort to account for these type *a* transitions. On the other hand, Lee *et al.*[7] demonstrated that these type *a* transitions arise quite naturally in a correct quantitative description of the direct molecular photoionization process itself and a polarization-induced autoionization mechanism need not be invoked. In their calculations, both type *a* and type *c* transitions are predicted in excellent agreement with the measured PFI spectra. They further attributed these type *a* transitions to odd partial wave (particularly the *p* wave) contributions to the photoelectron matrix element. These odd partial waves are entirely molecular in origin and arise from angular momentum coupling in photoelectron continua. Such coupling is clearly absent in an atomiclike picture.

In this paper, we investigate systematically the rotationally resolved ZEKE PFI spectra arising from the $1b_1$ orbitals of H_2O and D_2O. These studies are carried out using Hartree–Fock photoelectron molecular orbitals which account for the angular momentum coupling inherent in these electronic continnum states. Useful selection rules governing angular momentum changes ΔK_a and ΔK_c upon photoionization are derived and used in the analysis of these photoelectron spectra. To provide further insight into the photoionization dynamics, we also present photoelectron angular distributions.

II. THEORY AND NUMERICAL DETAILS

A. Differential cross section

Photoionization of the $1b_1$ orbital of the $\tilde{X}\,^1A_1$ ground state of H_2O (D_2O) leads to the $\tilde{X}\,^2B_1$ ground state of the ion. Under collision-free conditions, the rotationally resolved differential cross section for single-photon ionization of a rotational level of the ground state by linearly polarized light can be written as

[a] Permanent address: Departamento de Química, Universidade Federal de São Carlos Caixa Postal 676, CEP 13560 São Carlos, São Paulo, Brazil.
[b] Contribution No. 8606.

 0021-9606/92/173108-07$06.00

$$\frac{d\sigma}{d\Omega} \propto \sum_{M_{J_i} M_{J_+}} \rho_{M_{J_i} M_{J_i}} |\Gamma_{M_{J_i} M_{J_+}}|^2$$

$$= \frac{\sigma}{4\pi} [1 + \beta P_2(\cos\theta)], \tag{1}$$

where σ is the total cross section, β is the asymmetry parameter, $P_2(\cos\theta)$ is the Legendre polynominal, $\rho_{M_{J_i} M_{J_i}}$ is the population of the M_{J_i} sublevel of the ground state, and $|\Gamma_{M_{J_i} M_{J_+}}|^2$ is the ionization probability out of the M_{J_i} sublevel of the ground state leading to the M_{J_+} sublevel of the ion. The bound–free transition dipole matrix element $\Gamma_{M_{J_i} M_{J_+}}$ has been derived previously and has the form[8]

$$\Gamma_{M_{J_i} M_{J_+}} = \sum_{lm} C_{lm}(M_{J_i} M_{J_+}) Y_{lm}(\hat{k}'), \tag{2}$$

where

$$C_{lm}(M_{J_i} M_{J_+}) = \sqrt{\frac{4\pi}{3}} \frac{1}{2} [(2J_i + 1)(2J_+ + 1)(2N_i + 1)(2N_+ + 1)(2S_i + 1)]^{1/2} \sum (-1)^Q (2N_t + 1)$$
$$\times \begin{pmatrix} S_+ & 1/2 & S_i \\ M_{S_+} & m_\sigma & -M_{S_i} \end{pmatrix} \begin{pmatrix} N_+ & S_+ & J_+ \\ M_{N_+} & M_{S_+} & -M_{J_+} \end{pmatrix} \begin{pmatrix} N_i & S_i & J_i \\ M_{N_i} & M_{S_i} & -M_{J_i} \end{pmatrix}$$
$$\times \begin{pmatrix} N_+ & N_i & N_t \\ -M_{N_+} & M_{N_i} & m_t \end{pmatrix} \begin{pmatrix} N_t & 1 & l \\ -m_t & \mu_0 & m \end{pmatrix} a_{N_i \tau_i K_i} a_{N_+ \tau_+ K_+} \tilde{I}^{\gamma q}_{h l \lambda \mu}(\Lambda_f \Sigma_f) b^{\gamma q}_{h l \lambda}(\Lambda_f \Sigma_f)$$
$$\times [1 + (-1)^{\Delta p + \Delta N + l + 1}] \left[\begin{pmatrix} N_+ & N_i & N_t \\ -K_+ & K_i & K_t \end{pmatrix} \begin{pmatrix} N_t & 1 & l \\ -K_t & \mu & \lambda \end{pmatrix} + (-1)^{p_+} \right.$$
$$\left. \times \begin{pmatrix} N_+ & N_i & N_t \\ K_+ & K_i & K_t \end{pmatrix} \begin{pmatrix} N_t & 1 & l \\ -K_t & \mu & \lambda \end{pmatrix} \right], \tag{3}$$

$$Q = \Delta N + \Delta M_J - S_i + M_{S_i} - \mu_0 - m + M_{N_+} + K_i - 1/2, \tag{4}$$

$$\tilde{I}^{\gamma q}_{h l \lambda \mu}(\Lambda_f \Sigma_f) = \langle \gamma_+ q_+ \gamma_e q_e | \Lambda_f \rangle \langle M_{S_+} m_\sigma | \Sigma_f \rangle \times I^{\gamma q}_{h l \lambda \mu}(\Lambda_f \Sigma_f), \tag{5}$$

and

$$I^{\gamma q}_{h l \lambda \mu}(\Lambda_f \Sigma_f) = \sqrt{\frac{2}{\pi}} \frac{(-i)^l}{k} \int dR\, dr\, \psi^*_{+}(\mathbf{r},R) \times \chi^*_{v_+}(R) \phi^{*(-)\gamma q}_{h l \lambda}(\mathbf{r},R) r Y_{1\mu} \times \psi_i(\mathbf{r},R) \chi_{v_i}(R), \tag{6}$$

with $\Delta N = N_+ - N_i$, $\Delta p = p_+ - p_i$, $\Delta M_J = M_{J_+} - M_{J_i}$, and the summation in Eq. (3) goes over all possible indices. In these equations, ψ and χ_v are the electronic and vibrational wave functions, respectively, $\phi^{(-)\gamma q}_{h l \lambda}$ is a partial wave component of the photoelectron wave function, J is the total angular momentum, M_J is its projection in the laboratory frame, N is the total angular momentum apart from spin, M_N and K are its projections in the laboratory and molecular frames, respectively, S is the total spin, M_S is its projection in the laboratory frame, μ_0 and μ are the photon polarization indices in the laboratory and molecular frames, respectively, l is an angular momentum component of the photoelectron, and m and λ are the projections of l in the laboratory and molecular frames, respectively. Note that subscripts i and $+$ denote quantum numbers for the ground and ionic states, respectively. In Eq. (3), $a_{N\tau K}$ are the coefficients for the expansion of the asymmetric top wave functions which are determined by diagonalizing the rigid rotor Hamiltonian in the symmetric top basis.[8] p is the parity index for asymmetric top functions with the value of 0 or 1 (Refs. 8 and 9) and $b^{\gamma q}_{h l \lambda}$ are the coefficients for the expansion of generalized harmonics in the spherical harmonics basis.[10] In $b^{\gamma q}_{h l \lambda}$, γ is one of the irreducible representations (IR) of the molecular point group, q is a component of this representation, and h distinguishes between different bases for the same IR corresponding to the same value of l. Substituting Eq. (2) into Eq. (1), one obtains

$$\sigma \propto \sum_{\substack{lm \\ M_{J_i} M_{J_+}}} \rho_{M_{J_i} M_{J_i}} |C_{lm}(M_{J_i} M_{J_+})|^2 \tag{7}$$

and

$$\beta = \frac{5}{\sigma} \sum_{\substack{l l' m \\ M_{J_i} M_{J_+}}} (-1)^m (2l + 1)(2l' + 1) \rho_{M_{J_i} M_{J_i}} \times C_{lm}(M_{J_i} M_{J_+}) C^*_{l' m}(M_{J_i} M_{J_+}) \times \begin{pmatrix} l & l' & 2 \\ m & -m & 0 \end{pmatrix} \begin{pmatrix} l & l' & 2 \\ 0 & 0 & 0 \end{pmatrix}. \tag{8}$$

B. Parity selection rules

From Eq. (3), we obtain the general parity selection rule

$$\Delta N + \Delta p + l = \text{odd}, \tag{9}$$

which has the same form as for diatomic molecules for Hund's case (b) coupling.[11–14] Note that the parity index in Eq. (9) pertains to the symmetric top basis used in the ex-

pansion of the asymmetric top wave functions.[8] To make Eq. (9) more useful, its dependence on the angular momentum changes ΔK_a and ΔK_c, where $\Delta K_a = K_a^+ - K_a^i$ and $\Delta K_c = K_c^+ - K_c^i$ with K_a and K_c the projections of N along the principal axes a and c, respectively, must be made more transparent. With a choice of a left-handed coordinate system for the molecule-fixed x, y, and z axes and choosing the molecular z axis to be the symmetry axis, it can be shown[8] that ΔK_η is even (odd) when $\Delta N + \Delta p$ is even (odd), where η is the principal axis which lies along the molecular x axis and K_η is the projection of the total angular momentum along this axis. The parity selection rule of Eq. (9) then reduces to

$$\Delta K_\eta + l = \text{odd}. \tag{10}$$

Using the properties of 3-j symbols, the following additional selection rules can be derived from Eq. (3):

$$\mu + \lambda = \begin{cases} \Delta K_a, & \text{if } a \parallel z \parallel \text{ the symmetry axis} \\ \Delta K_b, & \text{if } b \parallel z \parallel \text{ the symmetry axis} \\ \Delta K_c, & \text{if } c \parallel z \parallel \text{ the symmetry axis} \end{cases}, \tag{11}$$

where μ and λ are defined below Eq. (6). To connect the selection rules of Eqs. (10) and (11), a relationship among ΔK_a, ΔK_b, and ΔK_c is essential. This relationship can be obtained from the symmetry properties of the asymmetric top[9]

$$\Delta K_a + \Delta K_c = \text{even(odd)} \leftrightarrow \Delta K_b = \text{even(odd)}. \tag{12}$$

Therefore, the determination of $\mu + \lambda$ becomes a crucial step in application of these selection rules. Although Eqs. (10)–(12) are suitable for any nonlinear polyatomic molecule, $\mu + \lambda$ has to be determined specifically for the particular molecular symmetry.

In these studies, the molecular z axis is chosen to coincide with the C_2 symmetry axis and the x axis lies in the plane of the molecule (ion). Thus, the molecular x, y, and z axes coincide with the a, c, and b axes, respectively, for H_2O (D_2O) and H_2O^+ (D_2O^+). From Eqs. (10)–(12), we now have

$$\Delta K_a + l = \text{odd} \tag{13}$$

and

$$\mu + \lambda = \Delta K_b. \tag{14}$$

For the C_{2v} point group of interest here, the x, y, and z components of the dipole moment operator belong to the b_2, b_1, and a_1 irreducible representations, respectively. There are three corresponding dipole-allowed continuum channels, namely ka_2, ka_1, and kb_1 for photoionization of the $1b_1$ orbital of the ground state H_2O (D_2O). In these cases, even λ and odd μ are associated with ka_1 and ka_2 continuum channels, whereas odd λ and even μ are associated with the kb_1 channel. Therefore, $\lambda + \mu$ is always odd for all the allowed transitions and hence

$$\Delta K_a + \Delta K_c = \text{odd}. \tag{15}$$

From Eqs. (13) and (15), we conclude that both type a (ΔK_a = even and ΔK_c = odd) and type c (ΔK_a = odd and ΔK_c = even) transitions are allowed, but type b [ΔK_a = even (odd) and ΔK_c = even (odd)] transitions are forbidden. Furthermore, Eq. (13) shows that type a transitions arise from odd partial wave contributions to the photoelectron matrix element, whereas type c transitions are due to even partial wave contributions.

Tonkyn *et al.*[4] have carried out simulations of these ZEKE-PFI photoelectron spectra assuming that type a and type c transitions arise from ka_2 and ka_1 photoelectron continua, respectively. This assumption disagrees with above selection rules and previous studies.[7] As pointed out by Lee *et al.*,[7] these type a transitions arise mainly from p partial waves of the ka_1 and kb_1 continua. The ka_2 continuum, dominated by the d partial wave with no p angular momentum component, should not be responsible for these type a transitions. We now show that this assumption is invalid. From the properties of C_{2v} symmetry, it can be shown that dipole-allowed transitions satisfy these symmetry relations

$$\Gamma_{\Psi_i^e} \otimes \Gamma_{T_\alpha} \otimes \Gamma_{\Psi_f^e} = A_1, \tag{16}$$

$$\Gamma_{\Psi_i^R} \otimes \Gamma_{R_\alpha} \otimes \Gamma_{\Psi_f^R} = A_1, \tag{17}$$

and

$$\Gamma_{T_\alpha} \otimes \Gamma_{R_\alpha} = A_2, \tag{18}$$

with $\alpha = x$, y, and z; T_α and R_α are the translational and rotational operators, respectively;[15] Ψ_i^e and Ψ_f^e are the electronic wave functions of the initial and final states, respectively; and Ψ_i^R and Ψ_f^R are the rotational parts of the initial- and final-state wave functions, respectively. Equation (16) shows that three dipole-allowed transitions ka_1, ka_2, and kb_1 are associated with $\Gamma_{T_x}(b_1)$, $\Gamma_{T_y}(b_2)$, and $\Gamma_{T_x}(a_1)$, respectively, for photoionization of a $1b_1$ orbital. From Eqs. (17) and (18), $\Gamma_{\Psi_i^R} \otimes \Gamma_{\Psi_f^R}$ has b_2, b_1, and a_2 symmetry for $\alpha = x$ (ka_1 continuum), y (ka_2 continuum), and z (kb_1 continuum), respectively. Note that in Eq. (17), the symmetry of the final state includes that of the ion and photoelectron, i.e., $\Gamma_{\Psi_f^R} = \Gamma_{\Psi_+^R} \otimes \Gamma_{\phi^R}$ with Ψ_+^R and ϕ^R the rotational parts of the ion and photoelectron wave functions in the laboratory frame, respectively. ϕ^R has the form[8] of $[(-1)^{\lambda-m} b^{\gamma q}_{hl\lambda} \mathscr{D}^l_{m\lambda} + (-1)^{-\lambda-m} b^{\gamma q}_{hl-\lambda} \mathscr{D}^l_{m-\lambda}]$ $Y_{lm}(\hat{k}')$ with $\mathscr{D}^l_{m\lambda}$ a rotational matrix in Edmonds's notation[16] and $Y_{lm}(\hat{k}')$ a spherical harmonic. Since Γ_{ϕ^R} can belong to any IR of C_{2v} symmetry, $\Gamma_{\Psi_+^R}$ can too for each $\Gamma_{\Psi_f^R}$ (restricted by $\Gamma_{\Psi_f^R} = \Gamma_{\Psi_+^R} \otimes \Gamma_{\phi^R}$). Again from the property of C_{2v} symmetry, it can be shown that the total symmetry of $\Gamma_{\Psi_i^R} \otimes \Gamma_{\Psi_+^R}$ can be b_1, b_2, a_2, and a_1, which correspond to type a, type c, type b, and type b transitions, respectively. Therefore, each allowed symmetry of $\Gamma_{\Psi_i^R} \otimes \Gamma_{\Psi_f^R}$, associated with a specific ionization channel, will provide four possible symmetries for $\Gamma_{\Psi_i^R} \otimes \Gamma_{\Psi_+^R}$, i.e., each continuum contributes to type a, type c, and type b transitions. For example, if $\Gamma_{\Psi_i^R} \otimes \Gamma_{\Psi_f^R} = b_2$ (ka_1 continuum), $\Gamma_{\Psi_i^R} \otimes \Gamma_{\Psi_+^R}$ belongs to b_2 (type c), b_1 (type a), a_2 (type b), and a_1 (type b) symmetries associated with $\Gamma_{\phi^R} = a_1$, a_2, b_1, and b_2, respectively. Note that type b transitions are forbidden once nuclear spin is considered. This conclusion differs from that of Tonkyn *et al.*[4] However, if the ϕ^R term shown above is not included in defining the photoelectron wave function as is the case for

bound–bound transitions (i.e., $\Gamma_{\psi_f^R} = \Gamma_{\psi_+^R}$), the conclusions of Tonkyn *et al.*[4] are readily obtained.

C. Calculational details

The ground state wave function of H_2O used here is obtained at the self-consistent-field (SCF) level at the equilibrium geometry[17] of $R(O\text{–}H) = 1.81a_0$ and $\theta(H\text{–}O\text{–}H) = 104.5°$. The basis set consists of a [5*s*4*p*] contraction of the (10*s*6*p*) primitive Cartesian Gaussian functions of Dunning,[18] augmented by two *s* ($\alpha = 0.028$ and 0.003), two *p* ($\alpha = 0.021$ and 0.002), and three *d* ($\alpha = 1.322$, 0.3916, and 0.09) functions on the oxygen atom. On the hydrogen atom, we used a [3*s*] contraction of the (4*s*) primitive Gaussian functions of Dunning,[18] augmented with one *s* ($\alpha = 0.05$) and two *p* ($\alpha = 1.12$ and 0.1296) functions. The total SCF energy in this basis was $-76.052\,376$ a.u., in good agreement with the HF limit of -76.066 a.u.[19]

The procedures for obtaining the photoelectron continuum orbitals used in these studies have been discussed previously.[20,21] Briefly, the photoelectron orbitals ϕ_k are obtained using an iterative procedure, based on the Schwinger variational principle,[22] to solve the Lippmann–Schwinger equation. This procedure begins by approximating the static-exchange (SE) potential of the molecular ion by a separable form

$$U_{\rm SE} \approx U_S(\mathbf{r},\mathbf{r}') = \sum_{ij} \langle \mathbf{r}|U|\alpha_i\rangle (U^{-1})_{ij} \langle \alpha_j|U|\mathbf{r}'\rangle, \tag{19}$$

where the matrix U^{-1} is the inverse of the matrix with elements $U_{ij} = \langle \alpha_i|U|\alpha_j\rangle$ and the α's are discrete basis functions such as Cartesian or spherical Gaussian functions. U is twice the static-exchange potential with the long-range Coulomb potential removed. The Lippmann–Schwinger equation with this separable potential $U_S(\mathbf{r},\mathbf{r}')$ can be readily solved yielding approximate photoelectron orbitals $\phi_k^{(0)}$. These solutions can be improved iteratively to yield converged solutions to the Lippmann–Schwinger equation containing the full static-exchange potential. In this study, four iterations provided converged results. The basis sets used in the separable expansion of Eq. (19) are listed in Table I.

All matrix elements arising in the solutions of the Lippmann–Schwinger equation were evaluated via single-center expansions about the center of mass. All angular momentum partial wave expansions were truncated at $l = 7$. These expansions give orbital integrals better than 0.99 for all bound orbitals. Increasing the maximum value of l in these expansions did not lead to any significant change in the resulting cross sections.

In these studies, we assume a rotational temperature of 15 K for jet-cooled H_2O and D_2O and 300 K for the room temperature species. Furthermore, we assume that there is no spin exchange taking place during the jet-cooled expansion of room-temperature water. Therefore, the *ortho* (antisymmetric) to *para* (symmetric) ratio for jet-cooled H_2O is 3:1 and 2:1 (symmetric/antisymmetric species) for D_2O. The relative population of rotational levels of the ground state of H_2O (D_2O) is determined by[23]

TABLE I. Basis sets used in the separable potential of Eq. (19).

Symmetry	Center	Cartesian Gaussian function[a]	Exponents (α)
a_1	O	*s*	16.0, 8.0, 4.0, 2.0, 1.0, 0.5, 0.25, 0.1
		z	4.0, 2.0, 1.0, 0.5, 0.1
		x^2	1.0, 0.5, 0.1
		y^2	1.0, 0.5, 0.1
		z^2	1.0, 0.5, 0.1
	H	*s*	2.0, 1.0, 0.5, 0.1
		x	0.5, 0.1
b_1	O	*y*	4.0, 2.0, 1.0, 0.5, 0.1
		yz	1.0, 0.1
	H	*y*	1.0, 0.5, 0.1
a_2	O	*xy*	8.0, 4.0, 2.0, 1.0, 0.5, 0.1, 0.03
	H	*y*	1.0, 0.5, 0.1

[a] $\phi^{\alpha,l,m,n,A}(\mathbf{r}) = \mathcal{N}(x-A_x)^l(y-A_y)^m(z-A_z)^n \exp(-\alpha|\mathbf{r}-\mathbf{A}|^2)$ with $\mathcal{N}$ a normalization constant.

$$\rho_{M_{J_i}M_{J_i}}(T) = \frac{(2J+1)}{Q_{\rm S,A}} \exp[-(E_{\rm rot} - E^0_{S,A})/k_B T], \tag{20}$$

where $E_{\rm rot}$ is the rotational energy, $E^0_{S,A}$ is the energy of the 0_{00} (symmetric) rotational level and the 1_{01} (antisymmetric) level, $Q_{\rm S,A}$ is the partition function for the symmetric and antisymmetric species, and k_B is the Boltzmann constant. This population distribution is further normalized to the statistical ratio as quoted above for the symmetric and antisymmetric species.

III. RESULTS AND DISCUSSION

Figure 1 shows the measured[4] and calculated rotationally resolved ZEKE photoelectron spectra for single-photon

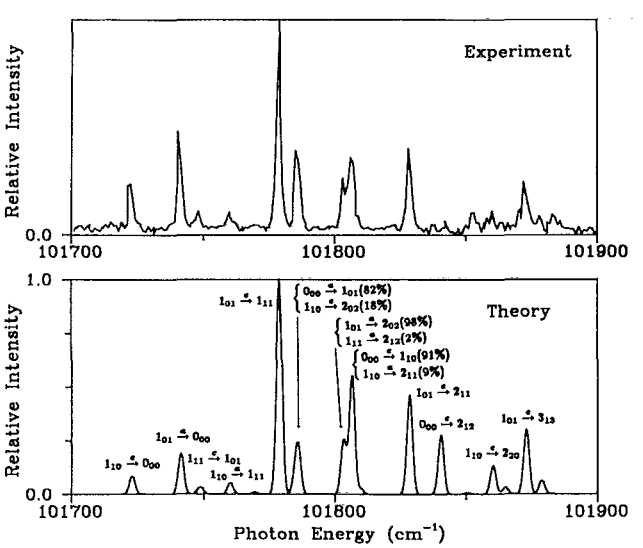

FIG. 1. The measured (top) and calculated (bottom) ion rotational distributions for photoionization of the $1b_1$ orbital of the $\tilde{X}\,^1A_1$ ground state of jet-cooled H_2O. The *a* and *c* labels indicate type *a* and type *c* transitions, respectively.

ionization of the $1b_1$ orbital of the $\tilde{X}\,^1A_1$ (000) state of jet-cooled H_2O leading to the $\tilde{X}\,^2B_1$ (000) state of H_2O^+. A photoelectron kinetic energy of 50 meV and a rotational temperature at 15 K are assumed in these calculations. The calculated spectra are convoluted with a Gaussian detection function having a full width at half-maximum (FWHM) of 1.5 cm^{-1}. The agreement between the calculated and measured spectra is very encouraging except for the calculated $0_{00} \rightarrow 2_{12}$ peak which is somewhat stronger than that of the measured value. The origin of this discrepancy is not clear. However, the calculated branching ratio for type *c* transitions originating from the 1_{01} rotational level of H_2O and leading to the 1_{11}, 2_{11}, and 3_{13} levels of H_2O^+ is 1.0:0.48:0.27 in good agreement with the measured ratio of 1.0:0.42:0.25.

According to the parity selection rules of Eqs. (13)–(15), type *a* transitions ($1_{01} \rightarrow 0_{00}$, $0_{00} \rightarrow 1_{01}$, $1_{01} \rightarrow 2_{02}$, and $1_{11} \rightarrow 2_{12}$) arise from odd (almost pure *p*) wave contributions to the photoelectron matrix element. These *p* partial waves of the ka_1 and kb_1 continua are entirely molecular in origin, since the almost pure *p* (99.7%) character of the $1b_1$ orbital would lead only to *s* and *d* (even) photoelectron continua in an atomiclike picture. Note that the ka_2 continuum makes almost no contribution to these type *a* transitions because the *f* (odd) wave is almost negligible. However, the type *c* transitions $1_{01} \rightarrow 1_{11}$, $1_{10} \rightarrow 0_{00}$, and $1_{10} \rightarrow 2_{20}$ have almost pure *s* wave contributions, while the $1_{01} \rightarrow 2_{11}$, $0_{00} \rightarrow 2_{12}$, and $1_{01} \rightarrow 3_{13}$ transitions have about equal *s* and *d* wave contributions, demonstrating that ionization into the *s* continuum is significant and cannot be neglected.[5,6]

The rotationally resolved photoelectron angular distributions of Fig. 2 most clearly reveal the underlying dynamics of these spectra. To illustrate this it is useful to look at the magnitudes of several important (l,λ) components $|D^{(-)}_{l\lambda}|$ of the incoming-wave normalized dipole amplitude at a photoelectron energy of 50 meV. These angular components (in atomic units) are 0.1848 (0,0), 0.1084 (1,0), 0.1474 (2,0), 0.4254 (2,2), 0.0271 (3,0), and 0.0480 (3,2) in the ka_1 ionization continuum; 0.2351 (1,1), 0.4886 (2,1), 0.0752 (3,1), and 0.0071 (3,3) in the kb_1 ionization continuum; and 0.3812 (2,2) and 0.0460 (3,2) in the ka_2 ionization continuum. Strong *d* ($l = 2$) wave components are seen clearly in every continuum. However, the photoelectron angular distributions do not show a predominant *d*-wave character in type *c* transitions, indicating that there is strong interference between various continua. Type *a* transitions essentially arise from the *p* waves in the ka_1 and kb_1 channels. These type *a* transitions are, hence, similar to the nonatomic-like transitions seen previously in resonance enhanced multiphoton ionization of excited states of diatomic molecules.[24] They arise from strong *l* mixing in the electronic continua due to the nonspherical ion potential.

The near-threshold photoelectron spectra for photoionization of the $\tilde{X}\,^1A_1$ (000) state of jet-cooled H_2O leading to the $\tilde{X}\,^2B_1$ (100) vibrationally excited state of H_2O^+ have also been reported by Tonkyn *et al.*[4] Since the angular momentum composition of the $1b_1$ orbital varies only slowly with internuclear distance and no Cooper minimum is predicted in the photoelectron matrix element,[20,21] the ion rotational distributions should not depend on the vibrational state.

Figure 3 shows the measured[4] and calculated rotationally resolved ZEKE photoelectron spectra for photoionization of the $1b_1$ orbital of the ground state of room temperature H_2O. The calculated spectra are convoluted with a Gaussian detection function with an FWHM of 2.0 cm^{-1}. The assignments of the peaks in both spectra are not given since these spectra are much more congested than those of jet-cooled water due to the broad population distribution of rotational levels in the ground state. The agreement here

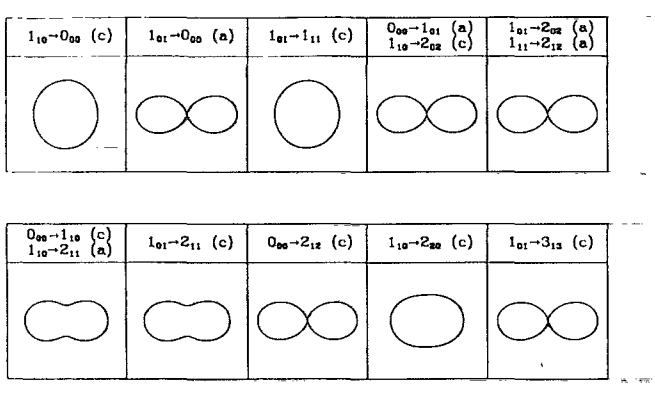

FIG. 2. The photoelectron angular distributions associated with specific rotational levels of Fig. 1. The *a* and *c* labels indicate type *a* and type *c* transitions, respectively. $\theta = 0°$ is vertical.

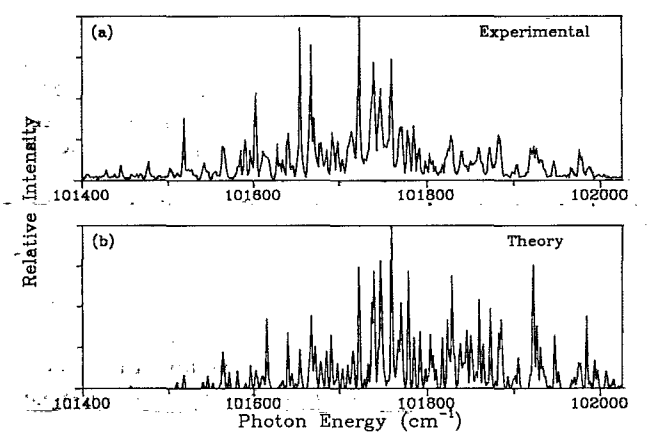

FIG. 3. The measured (top) and calculated (bottom) ion rotational distributions for photoionization of the $1b_1$ orbital of the $\tilde{X}\,^1A_1$ ground state of room temperature H_2O.

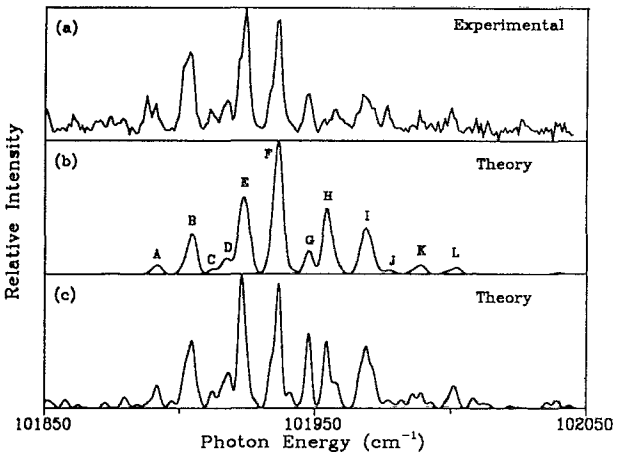

FIG. 4. The (a) experimental and (b) and (c) theoretical ion rotational distributions for photoionization of the $1b_1$ orbital of the $\tilde{X}\,^1A_1$ ground state of D_2O. The rotational transitions of each labeled peak are listed in Tables II and III for Figs. 4(b) and 4(c), respectively. See the text for an explanation.

between the calculated and measured spectra is less satisfactory than that of jet-cooled H_2O due to the high density of rotational transitions. However, all the observed transitions are accounted for in the calculated spectra. Note that peaks above 101 780 cm^{-1} in the observed spectra are systematically less intense than those in the calculated spectra. The reason for this trend is not clear.

Figure 4 shows the measured[4] [Fig. 4(a)] and calculated [Figs. 4(b) and 4(c)] rotationally resolved photoelectron spectra for photoionization of the $1b_1$ orbital of the ground state of jet-cooled D_2O. The calculated spectra are convoluted with a Gaussian detection function with an FWHM of 2.5 cm^{-1}. Since the photoelectron continuum is not expected to be influenced by isotopic substitution, these calculations use the same photoelectron matrix elements as for photoionization of H_2O. The spectra of Fig. 4(b) are calculated assuming a ratio of 1:2 for antisymmetric and symmetric species and a single rotational temperature at 15 K. For the spectra of Fig. 4(c), we assumed a nonequilibrated jet-cooled D_2O sample characterized by two rotational temperatures. We further assume temperatures of 15 and 100 K with relative populations of 0.7 and 0.3, respectively, for the symmetric species, and 0.9 and 0.1, respectively, for the antisymmetric species. Although we expect D_2O to be fully equilibrated in this free-jet expansion, particularly since the calculated and measured ion distributions of Fig. 1 certainly suggest that this is the case for H_2O, the excellent agreement between the measured distributions of Fig. 4(a) and the distributions of Fig. 4(c) suggests that the D_2O expansion may, in fact, not be equilibrated. The underlying mechanism for such behavior is certainly not clear to us, but we believe it is important to show these distributions. The dominant transitions associated with labeled peaks in Figs. 4(b) and 4(c) are listed in Tables II and III, respectively. In both tables, type *a* and type *c* transitions are seen and each peak has been normalized to unity (100%). As in the case of H_2O (Fig. 1), type *a* and type *c* transitions are present in both calculated and measured spectra.

TABLE II. Contributions to the peaks labeled in Fig. 4(b). Each peak has been normalized to unity (100%).

Peak	Transition	Type	Contribution
A	$1_{10} \rightarrow 0_{00}$	*c*	75.7
	$2_{02} \rightarrow 1_{01}$	*a*	17.2
	$2_{12} \rightarrow 1_{11}$	*a*	7.1
B	$1_{01} \rightarrow 0_{00}$	*a*	17.5
	$1_{11} \rightarrow 1_{01}$	*c*	70.5
	$2_{02} \rightarrow 1_{10}$	*c*	6.5
	$2_{12} \rightarrow 2_{02}$	*c*	5.5
C	$1_{10} \rightarrow 1_{11}$	*a*	100
D	$1_{11} \rightarrow 1_{10}$	*a*	56.4
	$2_{02} \rightarrow 2_{12}$	*c*	43.6
E	$0_{00} \rightarrow 1_{01}$	*a*	46.8
	$1_{01} \rightarrow 1_{11}$	*c*	45.7
	$1_{10} \rightarrow 2_{02}$	*c*	6.5
F	$0_{00} \rightarrow 1_{10}$	*c*	81.1
	$1_{01} \rightarrow 2_{02}$	*a*	7.1
	$1_{11} \rightarrow 2_{12}$	*a*	7.0
	$2_{02} \rightarrow 3_{03}$	*a*	1.9
G	$1_{01} \rightarrow 2_{11}$	*c*	88.7
	$2_{12} \rightarrow 2_{20}$	*c*	8.9
	$2_{11} \rightarrow 3_{12}$	*a*	2.4
H	$0_{00} \rightarrow 2_{12}$	*c*	81.5
	$1_{11} \rightarrow 3_{03}$	*c*	11.9
	$2_{02} \rightarrow 3_{12}$	*c*	6.6
I	$1_{01} \rightarrow 3_{13}$	*c*	21.1
	$1_{11} \rightarrow 2_{21}$	*c*	56.3
	$1_{10} \rightarrow 2_{20}$	*c*	20.4
	$2_{11} \rightarrow 3_{21}$	*c*	2.1
J	$1_{01} \rightarrow 2_{20}$	*a*	71.5
	$2_{12} \rightarrow 3_{22}$	*c*	28.5
K	$0_{00} \rightarrow 2_{21}$	*a*	100
L	$0_{00} \rightarrow 3_{12}$	*c*	39.5
	$1_{01} \rightarrow 3_{22}$	*a*	6.0
	$1_{11} \rightarrow 3_{21}$	*c*	37.9
	$1_{10} \rightarrow 3_{22}$	*c*	16.6

Figure 5 shows the photoelectron angular distributions associated with the labeled peaks of Fig. 4(b). Photoelectron angular distributions for the spectra of Fig. 4(c) are similar to those of Fig. 5 and are not shown. The dominant rotational transitions for these labeled peaks are shown in Table II. The photoelectron angular distributions of peaks *B* and *I*, which are dominated by type *c* transitions, have almost pure *s* wave contributions to the photoelectron matrix element, whereas those of peak *C*, dominated by type *a* transitions, have almost *p* wave contributions. However, the photoelectron angular distributions of other peaks reflect the mixture of even and odd partial wave contributions. Since the photoelectron matrix elements for D_2O and H_2O are assumed equal, the photoelectron angular distributions for the same rotational transition are expected to be the same. On the other hand, the photoelectron angular distributions of Fig. 5 behave quite differently from those of Fig. 2, indicating that interference between different rotational transitions is significant.

TABLE III. Contributions to the peaks labeled in Fig. 4(c). Each peak has been normalized to unity (100%).

Peak	Transition	Type	Contribution
A	$1_{10} \rightarrow 0_{00}$	*c*	70.2
	$3_{22} \rightarrow 3_{12}$	*c*	19.2
	$2_{21} \rightarrow 2_{11}$	*c*	2.0
	$2_{12} \rightarrow 1_{11}$	*a*	8.0
B	$2_{02} \rightarrow 1_{10}$	*c*	10.3
	$1_{01} \rightarrow 0_{00}$	*a*	14.2
	$3_{13} \rightarrow 3_{03}$	*c*	19.8
	$2_{12} \rightarrow 2_{02}$	*c*	6.7
	$1_{11} \rightarrow 1_{01}$	*c*	44.7
	$2_{11} \rightarrow 2_{12}$	*a*	2.0
C	$2_{20} \rightarrow 3_{03}$	*a*	3.9
	$3_{03} \rightarrow 3_{13}$	*c*	14.4
	$1_{10} \rightarrow 1_{11}$	*a*	81.6
D	$3_{13} \rightarrow 2_{21}$	*c*	8.2
	$1_{11} \rightarrow 1_{10}$	*a*	31.0
	$2_{02} \rightarrow 2_{12}$	*c*	59.4
	$2_{12} \rightarrow 2_{11}$	*a*	1.3
E	$3_{22} \rightarrow 3_{12}$	*c*	1.3
	$3_{13} \rightarrow 3_{12}$	*a*	1.1
	$1_{01} \rightarrow 1_{11}$	*c*	54.0
	$2_{20} \rightarrow 2_{21}$	*a*	5.3
	$2_{21} \rightarrow 2_{20}$	*a*	0.5
	$0_{00} \rightarrow 1_{01}$	*a*	20.0
	$1_{10} \rightarrow 2_{02}$	*c*	9.6
	$2_{20} \rightarrow 3_{12}$	*c*	2.1
	$2_{11} \rightarrow 3_{03}$	*c*	5.9
F	$1_{01} \rightarrow 2_{02}$	*a*	13.3
	$3_{31} \rightarrow 3_{30}$	*a*	2.8
	$1_{11} \rightarrow 2_{12}$	*a*	10.6
	$0_{00} \rightarrow 1_{10}$	*c*	55.1
	$1_{10} \rightarrow 2_{11}$	*a*	3.8
	$2_{02} \rightarrow 3_{03}$	*a*	7.2
	$2_{11} \rightarrow 2_{21}$	*c*	5.3
	$2_{12} \rightarrow 3_{13}$	*a*	1.7
G	$2_{11} \rightarrow 3_{21}$	*c*	9.8
	$1_{01} \rightarrow 2_{11}$	*c*	65.0
	$2_{12} \rightarrow 2_{20}$	*c*	9.6
	$3_{13} \rightarrow 3_{21}$	*c*	15.5
H	$2_{02} \rightarrow 2_{21}$	*a*	2.8
	$0_{00} \rightarrow 2_{12}$	*c*	52.6
	$2_{20} \rightarrow 3_{21}$	*a*	5.1
	$1_{11} \rightarrow 3_{03}$	*c*	11.9
	$2_{02} \rightarrow 3_{12}$	*c*	17.1
I	$1_{10} \rightarrow 2_{20}$	*c*	26.6
	$1_{11} \rightarrow 2_{21}$	*c*	47.8
	$1_{01} \rightarrow 3_{13}$	*c*	22.1
	$3_{22} \rightarrow 3_{30}$	*c*	3.4
J	$2_{11} \rightarrow 3_{21}$	*c*	69.0
	$1_{11} \rightarrow 3_{12}$	*a*	4.0
	$1_{01} \rightarrow 2_{20}$	*a*	26.9
K	$0_{00} \rightarrow 2_{21}$	*a*	76.3
	$2_{02} \rightarrow 3_{21}$	*a*	23.6
L	$0_{00} \rightarrow 3_{12}$	*c*	10.0
	$1_{10} \rightarrow 3_{22}$	*c*	14.5
	$3_{13} \rightarrow 3_{30}$	*a*	1.8
	$1_{11} \rightarrow 3_{21}$	*c*	21.6
	$2_{21} \rightarrow 3_{31}$	*c*	3.7
	$2_{20} \rightarrow 3_{30}$	*c*	44.3
	$1_{01} \rightarrow 3_{22}$	*a*	4.1

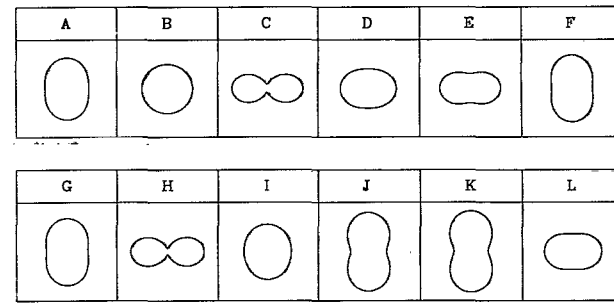

FIG. 5. The calculated photoelectron angular distributions associated with the labeled peaks of Fig. 4(b).

ACKNOWLEDGMENTS

This work was supported by grants from the National Science Foundation, Air Force Office of Scientific Research, and the Office of Health and Environmental Research of the U.S. Department of Energy. We also acknowledge use of resources of the Jet Propulsion Laboratory/Caltech CRAY Y-MP2E/116 Supercomputer. One of us (M. T. L.) thanks the Conselho Nacional de Desenvolvimento Científico e Tecnológico (CNPq, Brazil) for financial support.

[1] R. N. Compton and J. C. Miller, in *Laser Applications in Physical Chemistry*, edited by D. K. Evans (Dekker, New York, 1988).
[2] S. T. Pratt, P. M. Dehmer, and J. L. Dehmer, in *Advances in Multiphoton Processes and Spectroscopy*, edited by S. H. Lin (World Scientific, Singapore, 1988), and references therein.
[3] See K. Müller-Dethlefs and E. W. Schlag, Annu. Rev. Phys. Chem. **42**, 109 (1991), and references therein.
[4] R. G. Tonkyn, R. Wiedmann, E. R. Grant, and M. G. White, J. Chem. Phys. **95**, 7033 (1991).
[5] M. S. Child and Ch. Jungen, J. Chem. Phys. **93**, 7756 (1990).
[6] R. D. Gilbert and M. S. Child, Chem. Phys. Lett. **287**, 153 (1991).
[7] M.-T. Lee, K. Wang, V. McKoy, R. G. Tonkyn, R. T. Wiedmann, E. R. Grant, and M. G. White, J. Chem. Phys. **96**, 7848 (1992).
[8] M.-T. Lee, K. Wang, V. McKoy, and L. E. Machado, J. Chem. Phys. (in press).
[9] R. S. Mulliken, Phys. Rev. **59**, 873 (1941).
[10] P. G. Burke, N. Chandra, and F. A. Gianturco, J. Phys. B **5**, 2212 (1972).
[11] S. N. Dixit and V. McKoy, Chem. Phys. Lett. **128**, 49 (1986).
[12] K. Wang and V. McKoy, J. Chem. Phys. **95**, 4977 (1991).
[13] J. Xie and R. N. Zare, J. Chem. Phys. **93**, 3033 (1990).
[14] G. Raseev and N. Cherepkov, Phys. Rev. A **42**, 3948 (1990).
[15] J. T. Hougen, J. Chem. Phys. **37**, 1433 (1962).
[16] A. R. Edmonds, *Angular Momentum in Quantum Mechanics* (Princeton University, New Jersey, 1974).
[17] G. Herzberg, *Molecular Spectra and Molecular Structure III. Electronic Spectra and Electronic Structure of Polyatomic Molecules* (Van Nostrand, New York, 1966).
[18] T. H. Dunning, J. Chem. Phys. **55**, 716 (1971).
[19] T. H. Dunning, Jr., R. M. Pitzer, and S. Aung, J. Chem. Phys. **57**, 5044 (1972).
[20] M. Braunstein, V. McKoy, L. E. Machado, L. M. Brescansin, and M. A. P. Lima, J. Chem. Phys. **89**, 2998 (1988).
[21] L. E. Machado, L. M. Brescansin, M. A. P. Lima, M. Braunstein, and V. McKoy, J. Chem. Phys. **92**, 2362 (1990).
[22] R. R. Lucchese, G. Raseev, and V. McKoy, Phys. Rev. A **25**, 2572 (1982).
[23] H.-H. Kuge and K. Kleinermanns, J. Chem. Phys. **90**, 46 (1989).
[24] See, e.g., S. N. Dixit, D. L. Lynch, V. McKoy, and W. M. Huo, Phys. Rev. A **32**, 1267 (1985); H. Rudolph, V. McKoy, and S. N. Dixit, J. Chem. Phys. **90**, 2570 (1989); S. W. Allendorf, D. J. Leahy, D. C. Jacobs, and R. N. Zare, *ibid.* **91**, 2216 (1989); E. de Beer, C. A. de Lange, J. A. Stephens, K. Wang, and V. McKoy, *ibid.* **95**, 714 (1991); K. Wang, J. A. Stephens, and V. McKoy, *ibid.* **95**, 6456 (1991); K. Wang and V. McKoy, *ibid.* **95**, 7872 (1991).